What regulates electron injection in diffusive shock acceleration?

Siddhartha Gupta,[a,*] **Damiano Caprioli**[a,b] **and Anatoly Spitkovsky**[c]

[a]*Department of Astronomy and Astrophysics, University of Chicago, IL 60637, USA*

[b]*Enrico Fermi Institute, The University of Chicago, Chicago, IL 60637, USA*

[c]*Department of Astrophysical Sciences, Princeton University, 4 Ivy Ln., Princeton, NJ 08544, USA*

E-mail: gsiddhartha@uchicago.edu

Using fully kinetic particle-in-cell simulations, we study electron acceleration at non-relativistic quasi-parallel shocks for a wide range of shock speeds and magnetizations. We single out the necessary steps that lead to electron injection into diffusive shock acceleration and develop a minimal model that accounts for the trends observed in simulations. These scalings are key to understand the nonthermal phenomenology of a variety of heliophysical and astrophysical collisionless shocks.

ICRC2023
38th International Cosmic Ray Conference
The Astroparticle Physics Conference

*Speaker

1. Introduction

Cosmic rays (CRs) are the main ingredients behind the origin of high-energy observable such as gamma-rays, synchrotron X-rays, and radio which are produced by many astrophysical sources. Since the discovery of CRs, one of the main questions is how particles achieve this tremendous amount of energy that shows a power-law distribution over several decades in momentum/energy space. The pioneering work by Fermi [1] proposed that the particles can gain significant energy if they are repeatedly scattered by moving magnetic islands. [2–4] showed that collisionless shocks are environments in which particles can gain energy when diffusing back and forth across the shock. Such a diffusive shock acceleration (DSA) is supported by several observations at the Earth's bow shock [e.g., 5], at supernova and stellar cluster shocks [6–8], and in other galactic [e.g., 9] and extra-galactic environments [e.g., 10].

In the past decades, several important aspects of proton acceleration were thoroughly detailed in literature [see, e.g., 11–16]. Quasi-parallel shocks (with angle between the magnetic field and shock normal $\lesssim 50^o$) are very efficient proton accelerators, which is also consistent with observations [e.g., they account for the the bipolar gamma-ray morphology in SN1006, see 6, 12, 17]. Although electron acceleration has been also studied for several decades, the mystery of the acceleration mechanisms has not been solved. Since electrons are faster and involve scales much smaller than protons, identifying their acceleration mechanisms is both conceptually and numerically challenging. Only a few particle-in-cells (PIC) works reported the development of electron power-law tail in non-relativistic shocks [e.g., 18–24]. However, no theory fully explains *the conditions necessary for electrons to start DSA and what determines their injection fraction. These are the main objectives of our work.*

In this proceeding, we discuss our efforts to find the answers to the above questions (see also our upcoming paper, Gupta, Caprioli, Spitkovsky, in prep). The contents are organized as follows: the setup of our PIC simulations is outlined in §2, the main results are presented in §3 and summarized in §4.

2. Numerical Setup

We employ the massively parallel fully kinetic electromagnetic PIC code `Tristan-MP` [25] to simulate collisionless shocks. Our simulations are performed in the upstream rest frame, where the left boundary acts as a piston and the right one as the upstream free-escape boundary. To save computational time, such a boundary expands with time, up to $\approx 10^4 \, d_i$ for a typical run-time of $\sim 200 \, \omega_{ci}^{-1}$, where d_i and ω_{ci} denote the skin depth and the cyclotron frequency for the upstream ions respectively. For all runs the grid spacing is $\Delta x = d_e/10$, the time stepping is $\Delta t = 0.045 \omega_{pe}^{-1}$, and we use 200 particle per cell per species. The upstream plasma is set as Maxwellian for both electrons and ions. The magnetic field is defined by the Alfvénic speed ($v_A = B_0/\sqrt{4\pi n_0 m_i}$) and its inclination relative to shock normal is initialized to $\theta_{Bn} = \cos^{-1}(B_x/|\mathbf{B}_0|) = 30^o$ and is assumed to be in the $x - y$ plane. The shock is parameterized by the shock speed ($v_{sh} \approx 4/3 v_{pt}$, where v_{pt} is the piston speed), the Alfvénic Mach number ($\mathcal{M}_A = v_{sh}/v_A$), and the ion sonic Mach number ($\mathcal{M}_s = v_{sh}/v_{thi}$, where $v_{thi} = \sqrt{k_B T_i/m_i}$ denotes the thermal speed of the upstream ions). The corresponding electron sonic Mach number ($\mathcal{M}_{s,e}$) depends on the proton-to-electron mass-ratio
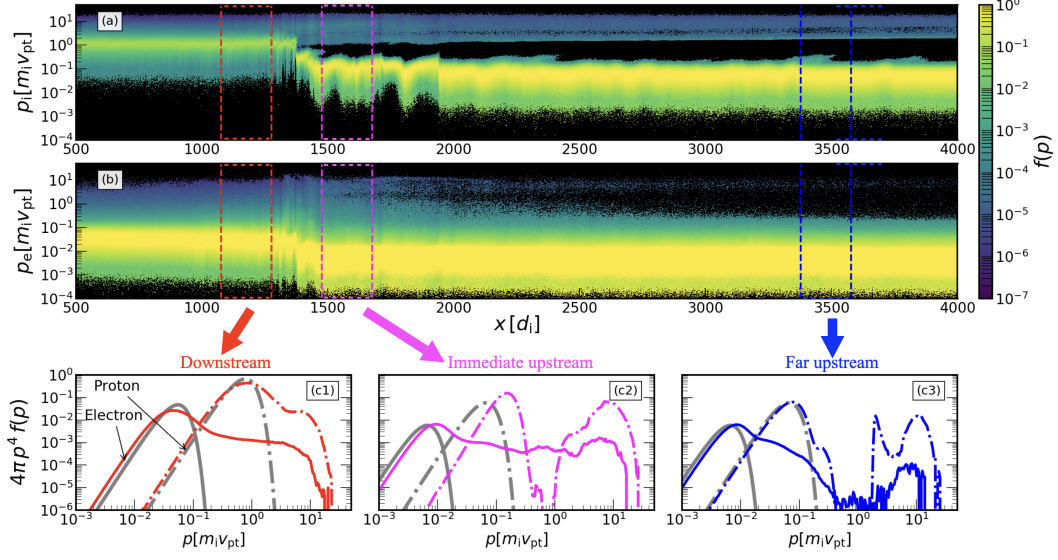
Figure 1: $x - |p|$ phase-space for protons (panel a) and electrons (panel b), and local spectra (panels c1–c3) for our benchmark shock simulation ($v_{pt}/c = 0.1$, $\mathcal{M}_A = 20$, $\mathcal{M}_s = 40$, and $m_R = 100$) at $t = 275\,\omega_{ci}^{-1}$.

that we adopt, $m_R = m_i/m_e$, i.e., $\mathcal{M}_{s,e} = \mathcal{M}_s/\sqrt{m_R}$. The plasma β, i.e., the ratio of thermal pressure ($P_{th} = \rho v_{th}^2$) to magnetic pressure ($P_B = B^2/8\pi$), spans the range $0.0625 - 16$.

3. Results

3.1 Momentum/energy distribution

Figure 1 shows the snapshot of the particle distribution of our benchmark run ($v_{pt}/c = 0.1$, $\mathcal{M}_A = 20$, $\mathcal{M}_s = 40$, and $m_R = 100$). Panels (a) and (b) represent the $x - p$ phase-space distribution of protons and electrons, which show the coexistence of the thermal and the energetic populations. These energetic populations are developed self-consistently in our simulations and characterization of their acceleration mechanisms is the main aim of our work. Panels (c1)–(c3) display the spectra of protons (dash-dotted line) and electrons (solid line) in the three different regions marked in panels (a) and (b). In panel (c1), the grey lines represent the thermal distribution of downstream plasma, which is obtained from the hydrodynamic shock jump conditions by assuming equipartition between electrons and protons [26]. The grey lines in panels (c2) and (c3) display the thermal Maxwellian distribution of far upstream plasma, as set by the sonic Mach number. Note that the horizontal axes in panels (c1)–(c3) are normalized to proton mass times the piston speed.

The downstream spectra (panel c1) clearly show a power-law tail $f(p) \sim p^{-4}$ attached to the Maxwellian distribution for both species, similar to what is reported in the literature [e.g., 20, 24, 27]. The immediate-/far-upstream spectra contain more complex features due to mixing among the return current, shock-reflected, and escaping particles. While both spectra show a nonthermal power-law distribution, it is not self-evident whether electrons are undergoing DSA. Moreover, since their power-law tail starts well below the proton nonthermal tail, it is naturally to

ask: do electrons need to have the same injection momentum as protons to participate in DSA? Our aim is to answer this question in our upcoming paper (Gupta, Caprioli, Spitkovsky, in prep).
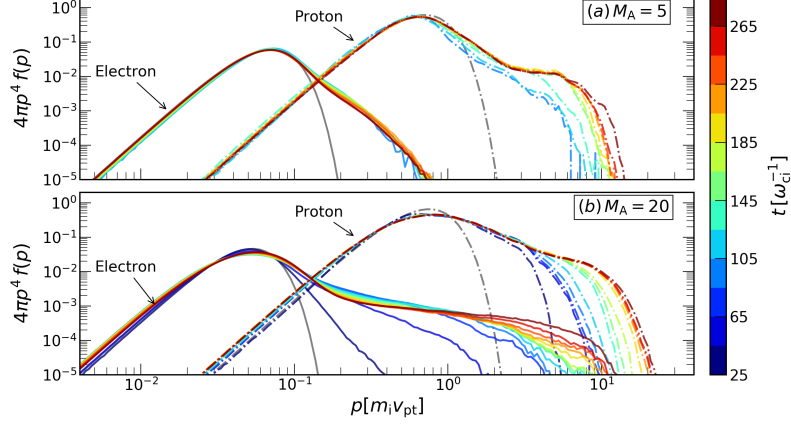
Figure 2: Comparison of downstream electron and proton spectra between $\mathcal{M}_A = 5$ (panel a) and $\mathcal{M}_A = 20$ (panel b) shocks.
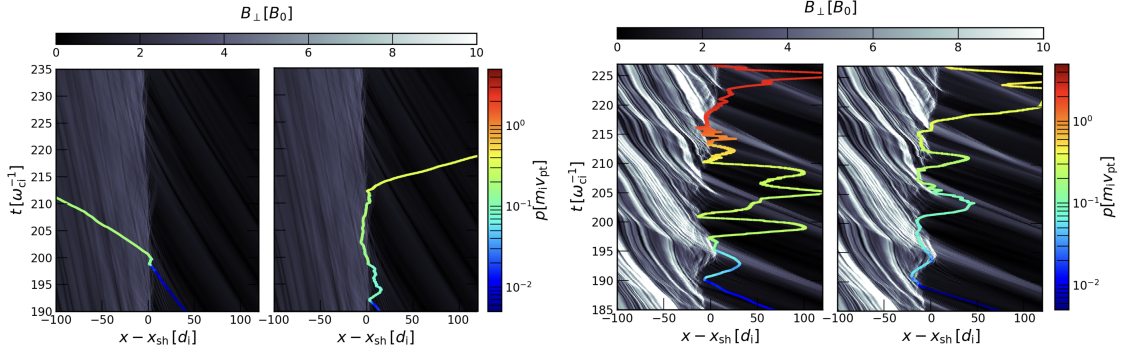
Figure 3: Typical trajectory of electrons for $\mathcal{M}_A = 5$ (left-most two panels) and $\mathcal{M}_A = 20$ (right-most two panels). The background colors show the space-time evolution of $B_\perp = \sqrt{B_y^2 + B_z^2}$ normalized to the initial magnetic field, B_0. The electron trajectories are color coded with their momentum (right color bars). In low-$\mathcal{M}_A$ shocks, electrons leave the accelerating region, whereas in high-$\mathcal{M}_A$ shocks, they scatter repetitively on the self-generated turbulence and their energy/momentum keeps increasing.

3.2 Dependence on shock parameters

To study the dependence of electron acceleration on different shock parameters such as the shock speeds, Alfvénic Mach numbers, and sonic Mach numbers, we vary only one parameter for a given run. Here we illustrate our numerical experiments using the example of two different scenarios, where we tune either Alfvénic Mach numbers (Figure 2) or sonic Mach numbers (Figure 4), for fixed $v_{pt}/c = 0.1$ and $m_R = 100$.

In Figure 2, panels (a) and (b) show the time evolution of the downstream spectra of electrons and protons for $\mathcal{M}_A = 5$ and $\mathcal{M}_A = 20$ shocks, respectively. While in both panels the extended tail beyond the thermal distribution (marked by grey curves) provides evidence of the accelerated electrons (solid curves) and protons (dash-dotted curves), we find that the nonthermal electron

distribution is comparatively softer (i.e., steeper) for $\mathcal{M}_A = 5$ than for $\mathcal{M}_A = 20$. To increase their energy, particles must remain close to the shock, which is guaranteed if strong turbulence is present, i.e., if $\delta B/B \gtrsim 1$. As the growth rate of the streaming instabilities increases with $\mathcal{M}_A$, the self-generated turbulence develops slowly in low-$\mathcal{M}_A$ shocks [e.g., 13, 28–30]. Moreover, the effective $\delta B/B_0$ that determines diffusivity and confinement of the particles is smaller for $\mathcal{M}_A = 5$, which results in the smaller extent of the spectrum. Also, analyzing the trajectory of individual electrons in our PIC simulations supports this reduced electron confinement for lower $\mathcal{M}_A$ (see Figure 3).

Next, we show the dependence on the sonic Mach number (Figure 4). Panels (a) to (c) show the downstream electron spectra for $\mathcal{M}_s = 10$, 40, and 160, respectively. All three runs provide evidence of nonthermal electrons, with an injection efficiency that gets smaller for decreasing $\mathcal{M}_s$, i.e., as one moves from panel (c) to panel (a). One may suspect that electron injection into DSA may depend, among other effects, on their upstream distribution being sub/supersonic, since a subsonic population should have an easier time crossing the shock in both directions. For the mass ratio used in these runs ($m_R = 100$), electrons are not supersonic in case of $\mathcal{M}_s = 10$ shock, however, they still manage to develop a nonthermal tail. The crucial role of electron sonic Mach number will be discussed in our forthcoming works (Gupta, Caprioli, Spitkovsky, in prep).
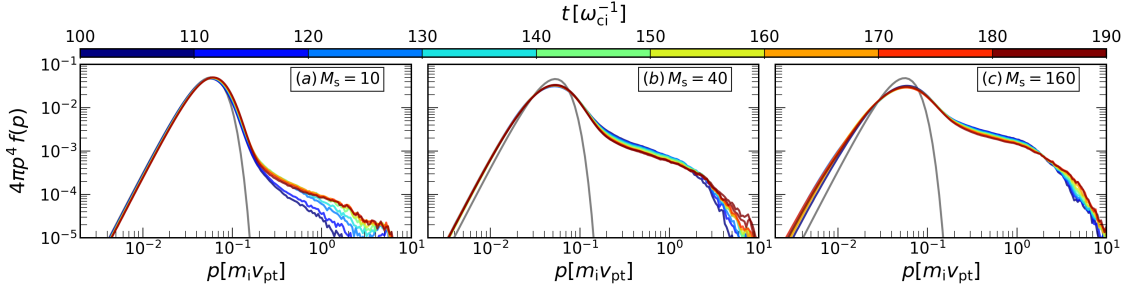
Figure 4: Downstream electron spectra for $\mathcal{M}_s = 10, 40$, and 60 shocks (the corresponding electron sonic Mach numbers $\mathcal{M}_{s,e} = 1, 4$, and 16 respectively). For these runs, $v_{pt}/c = 0.1$, $\mathcal{M}_A = 20$ and $m_R = 100$. The plasma β parameter for these runs is 16, 1, and 0.0625, respectively (from panel a to panel c).

4. Summary

We have performed a survey of fully kinetic 1D PIC simulations to study electron acceleration at quasi-parallel non-relativistic shocks for different speeds, Alfvénic Mach numbers ($\mathcal{M}_A$), and sonic Mach numbers ($\mathcal{M}_s$). Our primary focuses are to identify the threshold condition for electron DSA, characterize the evolution of the nonthermal tail, and quantify the acceleration efficiency for different shock parameters. We find that quasi-parallel shocks are good at accelerating both electrons and protons (Figure 1), which supports the previous findings reported in the literature [e.g., 20, 27]. We thoroughly explore how the upstream conditions and the proton-to-electron mass ratio control the electron acceleration efficiency. While the proton DSA efficiency is found to be quantitatively similar in different shock environments, we find that the electron DSA efficiency is quite sensitive to such parameters. In high Mach number shocks ($\mathcal{M}_A \gtrsim 10$), the electron DSA injection efficiency is about 1%, and the maximum energy increases due to the electromagnetic turbulence self-generated

by nonthermal protons (Figure 3). On the other hand, we find that the acceleration is slower in low Mach number shocks (Figure 2). Our results also suggest that high plasma-β shocks ($\beta \sim 10$) can inject fresh electrons into DSA (Figure 4), which has crucial implications in studies of galaxy cluster [18].

The ultimate aim of our study, of which only a small part is summarized here, is not just to provide a coherent description of electron DSA but also to develop a prescription that can be used to interpret non-thermal radio, X-rays, and $\gamma-$ray emissions from astrophysical sources in galactic and extragalactic environments. The results summarized in this proceeding will be reported in our upcoming papers (Gupta, Caprioli, Spitkovsky, in prep).

ACKNOWLEDGMENTS

References

[1] E. Fermi, *Galactic Magnetic Fields and the Origin of Cosmic Radiation.*, *Ap. J.* **119** (1954) 1.

[2] W.I. Axford, E. Leer and G. Skadron, *Acceleration of Cosmic Rays at Shock Fronts (Abstract)*, in Acceleration of Cosmic Rays at Shock Fronts, vol. 2 of *International Cosmic Ray Conference*, pp. 273–+, 1977, http://adsabs.harvard.edu/abs/1977ICRC....2..273A.

[3] A.R. Bell, *The non-linear self-regulation of cosmic ray acceleration at shocks*, *MNRAS* **225** (1987) 615.

[4] R.D. Blandford and J.P. Ostriker, *Particle acceleration by astrophysical shocks*, *ApJL* **221** (1978) L29.

[5] T.Z. Liu, V. Angelopoulos and S. Lu, *Relativistic electrons generated at Earth's quasi-parallel bow shock*, *Science Advances* **5** (2019) eaaw1368.

[6] F. Acero et al., *First detection of VHE γ-rays from SN 1006 by HESS*, *A&A* **516** (2010) A62+ [1004.2124].

[7] F. Aharonian, R. Yang and E. de Oña Wilhelmi, *Massive stars as major factories of Galactic cosmic rays*, *Nature Astronomy* **3** (2019) 561 [1804.02331].

[8] S. Gupta, B.B. Nath and P. Sharma, *Constraining cosmic ray acceleration in young star clusters using multi-wavelength observations*, *MNRAS* **479** (2018) 5220 [1804.05877].

[9] M. Su, T.R. Slatyer and D.P. Finkbeiner, *Giant Gamma-ray Bubbles from Fermi-LAT: Active Galactic Nucleus Activity or Bipolar Galactic Wind?*, *ApJ* **724** (2010) 1044 [1005.5480].

[10] R.J. van Weeren, H.J.A. Röttgering, M. Brüggen and M. Hoeft, *Particle Acceleration on Megaparsec Scales in a Merging Galaxy Cluster*, *Science* **330** (2010) 347 [1010.4306].

[11] L. Gargaté and A. Spitkovsky, *Ion Acceleration in Non-relativistic Astrophysical Shocks*, *ApJ* **744** (2012) 67 [1107.0762].

[12] D. Caprioli and A. Spitkovsky, *Simulations of Ion Acceleration at Non-relativistic Shocks: I. Acceleration Efficiency*, *ApJ* **783** (2014) 91 [1310.2943].

[13] D. Caprioli and A. Spitkovsky, *Simulations of Ion Acceleration at Non-relativistic Shocks: II. Magnetic Field Amplification*, *ApJ* **794** (2014) 46 [1401.7679].

[14] D. Caprioli and A. Spitkovsky, *Simulations of Ion Acceleration at Non-relativistic Shocks. III. Particle Diffusion*, *ApJ* **794** (2014) 47 [1407.2261].

[15] C.C. Haggerty and D. Caprioli, *Kinetic Simulations of Cosmic-Ray-modified Shocks. I. Hydrodynamics*, *ApJ* **905** (2020) 1 [2008.12308].

[16] D. Caprioli, C.C. Haggerty and P. Blasi, *Kinetic Simulations of Cosmic-Ray-modified Shocks. II. Particle Spectra*, *ApJ* **905** (2020) 2 [2009.00007].

[17] G. Winner, C. Pfrommer, P. Girichidis, M. Werhahn and M. Pais, *Evolution and observational signatures of the cosmic ray electron spectrum in SN 1006*, *MNRAS* **499** (2020) 2785 [2006.06683].

[18] X. Guo, L. Sironi and R. Narayan, *Non-thermal electron acceleration in low mach number collisionless shocks. i. particle energy spectra and acceleration mechanism*, *ApJ* **794** (2014) 153 [1406.5190].

[19] X. Guo, L. Sironi and R. Narayan, *Non-thermal electron acceleration in low mach number collisionless shocks. ii. firehose-mediated fermi acceleration and its dependence on pre-shock conditions*, *ApJ* **797** (2014) 47 [1409.7393].

[20] J. Park, D. Caprioli and A. Spitkovsky, *Simultaneous Acceleration of Protons and Electrons at Nonrelativistic Quasiparallel Collisionless Shocks*, *Physical Review Letters* **114** (2015) 085003 [1412.0672].

[21] P. Crumley, D. Caprioli, S. Markoff and A. Spitkovsky, *Kinetic simulations of mildly relativistic shocks: Particle acceleration in high mach number shocks*, *MNRAS* **485** (2019) 5105 [1809.10809].

[22] A. Bohdan, J. Niemiec, M. Pohl, Y. Matsumoto, T. Amano and M. Hoshino, *Kinetic Simulations of Nonrelativistic Perpendicular Shocks of Young Supernova Remnants. I. Electron Shock-surfing Acceleration*, *ApJ* **878** (2019) 5 [1904.13153].

[23] R. Xu, A. Spitkovsky and D. Caprioli, *Electron Acceleration in One-dimensional Nonrelativistic Quasi-perpendicular Collisionless Shocks*, *ApJL* **897** (2020) L41 [1908.07890].

[24] M. Shalaby, R. Lemmerz, T. Thomas and C. Pfrommer, *The Mechanism of Efficient Electron Acceleration at Parallel Nonrelativistic Shocks*, *ApJ* **932** (2022) 86 [`2202.05288`].

[25] A. Spitkovsky, *Simulations of relativistic collisionless shocks: shock structure and particle acceleration*, in *Astrophysical Sources of High Energy Particles and Radiation*, T. Bulik, B. Rudak and G. Madejski, eds., vol. 801 of *American Institute of Physics Conference Series*, pp. 345–350, Nov., 2005, DOI [`astro-ph/0603211`].

[26] F.H. Shu, *The physics of astrophysics. Volume II: Gas dynamics.* (1992).

[27] B. Arbutina and V. Zeković, *Non-linear diffusive shock acceleration: A recipe for injection of electrons*, *Astroparticle Physics* **127** (2021) 102546 [`2012.15117`].

[28] A.R. Bell, *Turbulent amplification of magnetic field and diffusive shock acceleration of cosmic rays*, *MNRAS* **353** (2004) 550.

[29] M.A. Riquelme and A. Spitkovsky, *Nonlinear Study of Bell's Cosmic Ray Current-Driven Instability*, *ApJ* **694** (2009) 626 [`0810.4565`].

[30] S. Gupta, D. Caprioli and C.C. Haggerty, *Lepton-driven Nonresonant Streaming Instability*, *ApJ* **923** (2021) 208 [`2106.07672`].